# High-Ampacity Power Cables of Tightly-Packed and Aligned Carbon Nanotubes

*Xuan Wang, Natnael Behabtu, Colin C. Young, Dmitri E. Tsentalovich, Matteo Pasquali, and Junichiro Kono**

**The current-carrying capacity (CCC), or ampacity, of highly-conductive, light, and strong carbon nanotube (CNT) fibers is characterized by measuring their failure current density (FCD) and continuous current rating (CCR) values. It is shown, both experimentally and theoretically, that the CCC of these fibers is determined by the balance between current-induced Joule heating and heat exchange with the surroundings. The measured FCD values of the fibers range from $10^7$ to $10^9$ A m$^{-2}$ and are generally higher than the previously reported values for aligned buckypapers, carbon fibers, and CNT fibers. To the authors' knowledge, this is the first time the CCR for a CNT fiber has been reported. The specific CCC value (i.e., normalized by the linear mass density) of these CNT fibers are demonstrated to be higher than those of copper.**

## 1. Introduction

Advanced materials utilizing carbon nanotubes (CNTs) are emerging. Recently, we reported a macroscopic fiber composed of tightly packed and well-aligned CNTs, which combines specific strength, stiffness, and thermal conductivity of carbon fibers with the specific electrical conductivity of metals ("specific": normalized by the linear mass density).[1] These macroscopic CNT fibers hold the promise to replace traditional metals for many applications including making stronger and lighter power transmission cables or electronic interconnections,[2] as well as durable field emission or thermionic emission sources.[3,4] These applications require the fiber to operate under high current, which leads to natural questions about the fiber's ability to carry such a current without being damaged. Traditionally, current carrying capacity (CCC), or often called ampacity, is used to quantify this ability. CCC is defined as the maximum amount of current a cable (including any insulating layer) can carry before immediate or progressive damages; sometimes, it is more convenient to use the current density, especially when making comparisons among different types of cables. Also, for weight-critical applications, for instance, in the aerospace industry, specific CCC (CCC normalized by the linear mass density) is usually considered.

Owing to the strong C–C bond, the CCC of individual CNTs can exceed $10^{13}$ A m$^{-2}$ without damage by electromigration,[5–7] which is 2 to 3 orders of magnitude greater than the electromigration limit of copper.[8] However, such superb CCC (limited by intrinsic optical phonon emission) becomes unapproachable when many CNTs are packed together to form a macroscopic CNT fiber or bundle. The unavoidable inter-tube transport significantly increases the resistivity, and the resultant Joule heating at high current densities raises the temperature, inducing damages and ultimately breaking the fiber. Thus, the competition between current-induced Joule heating and cooling by thermal environments becomes the determinant of the CCC, as in metal cables; this competition scales with the volume-to-surface ratio, which increases with increasing cable diameter, making Joule heating progressively more problematic for larger diameter cables.

So far, the most widely studied case for CNT networks is their immediate breakdown (usually in seconds or less) when carrying high current. The damage usually initiates around the hottest spot, particularly if associated with defects, kinks, or impurities.[9–12] The corresponding current limit can be defined as the failure current density (FCD), similar to the fuse current limit for metal cables. On the other hand, to be used as a power cable, CNT wires must operate below a regulations-specified

X. Wang, J. Kono
Department of Electrical and Computer Engineering
Rice University
Houston, TX 77005, USA
E-mail: kono@rice.edu
X. Wang, M. Pasquali, J. Kono
The Richard E. Smalley Institute for
Nanoscale Science and Technology
Rice University
Houston, TX 77005, USA
N. Behabtu, C. C. Young, D. E. Tsentalovich, M. Pasquali
Department of Chemical and Biomolecular Engineering
Rice University
Houston, TX 77005, USA
M. Pasquali
Department of Chemistry
Rice University
Houston, TX 77005, USA
M. Pasquali, J. Kono
Department of Materials Science and NanoEngineering
Rice University
Houston, TX 77005, USA
J. Kono
Department of Physics and Astronomy
Rice University
Houston, TX 77005, USA

**DOI: 10.1002/adfm.201303865**

© 2014 WILEY-VCH Verlag GmbH & Co. KGaA, Weinheim

temperature called the "operating temperature" ($T_o$) to avoid damaging its own insulation layer or other nearby accessories. The corresponding current limit is defined as the continuous current rating (CCR).[13] Since $T_o$ cannot be high enough to cause any damages, CCR is always much lower than the failure current. In contrast to metal power cables, whose CCR is well studied[14] and regulated,[13] so far no systematic study of these quantities for CNT wires is available.

Here, we determined both FCD and CCR for CNT fibers under various test conditions. We first measured the FCDs of those fibers. We monitored how the resistivity of the fiber under test evolved as a function of current density and found four distinct regimes. The measured FCDs varied from $10^7$ to $10^9$ A m$^{-2}$, depending on the dimensions of those fibers and test conditions. In particular, the measured FCD in vacuum was much lower than in gases due to a lack of heat exchange by gases, while the measured FCD in air was smaller than in the other tested gases because of oxidation. We then analyzed the heat exchange between CNT fibers and each type of gas and extracted the thermal conductance ($g$) between them. We proved that the heat exchange is governed by natural convection. In addition, we showed that due to tight packing and good alignment, gas molecules do not penetrate the body of the CNT fibers. When $g$ is known, any thermally determined CCC can be deduced if the corresponding temperature limit is given, and vice versa. As an example, we determined CCR for infinitely long CNT fibers with an operating temperature of 363 K.

Based on these measurements and heat-exchange analysis, we were able to make a comprehensive comparison of CCC with other cables. We showed that the FCD of our fibers was higher than previously reported carbon fibers and CNT fibers. We then compared these two parameters with a pure copper wire. Both the FCD and CCR of copper were still higher than CNT fibers mainly due to copper's lower resistivity. However, when normalized by the mass density, both specific FC (SFC) and CCR of copper wire were lower than those of these lightweight CNT fibers. Considering the fact that commercial transmission cables usually require extra reinforcement by a steel core because of copper's heavier weight and lower tensile strength, the combination of higher specific CCC and stronger mechanical strength of CNT fibers makes them promising candidates for transmission cables.

## 2. Results and Discussion

### 2.1. Determination of Failure Current Density in Vacuum

**Figure 1**a shows the resistivity versus temperature for the three highly-conductive CNT fibers[1] we studied, together with that for the reference copper wire with a diameter of 25.4 µm. The fibers we tested were electrically p-doped by the presence of sulfur and chlorine inside the fiber, which is a residuum from the chlorosulfonic acid solvent used in the fabrication of the fibers. The heavily acid-doped fiber contained more acid, making them less resistive. The room temperature resistivity for the heavily acid-doped fiber was about $2.57 \times 10^{-7}$ Ω m while that of the 10.5 µm diameter (20.5 µm diameter) acid-doped fiber was 4.12 (3.98) $\times 10^{-7}$ Ω m. On the other hand, the mass density of the heavily acid-doped sample was $1.5 \times 10^3$ kg m$^{-3}$, as compared to $1.2 \times 10^3$ kg m$^{-3}$ of the other acid-doped fibers. The room temperature resistivity of copper is approximately one order of magnitude less than that of fibers. Its accepted value is $1.725 \times 10^{-8}$ Ω m while the measured value here was $1.74 \times 10^{-8}$ Ω m. In all cases, the resistivity ($\rho$) linearly increased with temperature ($T$), that is,

$$\rho(T) = \rho(T_{\text{amb}})(1 + \alpha \cdot \Delta T), \tag{1}$$

where $T_{\text{amb}}$ is the ambient temperature, $\Delta T \equiv T - T_{\text{amb}}$ is the temperature measured from $T_{\text{amb}}$, and $\alpha$ is a positive constant. This equation provides us with a convenient means for monitoring the temperature rise as a result of current-induced heating.

Figure 1b shows the resistivity as a function of current density for the 20-µm-diameter acid-doped fiber in vacuum for $T_{\text{amb}} = 303$ K. The resistivity is normalized to the initial value, $\rho_0 = 3.98 \times 10^{-7}$ Ω m, before the fiber is heated. As the current density increases, the temperature increases through Joule heating, which in turn increases the resistivity through Equation 1. Starting from the lowest red curve, after a number of current-sweeping cycles, the resistivity versus current density curve undergoes irreversible changes with uneven paces. To better visualize this process, Figure 1c plots the highest applied current density in each current-sweeping cycle against the resistivity measured at a very low current density after the cycle [along the vertical dot-dashed line in Figure 1b].

Interestingly, Figure 1c reveals four distinct regimes as the current density is gradually increased from zero toward the ultimate value at which the fiber eventually breaks. In Regime 1, the *I–V* curve is reversible, and thus, the resistivity does not change after each sweeping cycle. In Regime 2, a drastic irreversible process takes place, and the resistivity permanently increases by about 4 times. In Regime 3, the I-V curve becomes reversible again, showing stable properties of a new, current-annealed fiber; that is, the acid, which is an effective dopant, is removed by heating. Finally, in Regime 4, the resistivity starts increasing very rapidly until the fiber breaks. Given sufficient time, any current–density value in Regime 4 ultimately leads to fiber breaking.

We define the current–density value that corresponds to the boundary between Regimes 3 and 4 as the failure current density, or FCD, of the fiber, which is different from the maximum current density before breaking (MCDBB) [see Figure 1c for the difference between FCD and MCDBB]. The value of MCDBB is ill-defined and can have a large uncertainty, depending on such experimental details as the sweeping speed, step size, sweeping method (current or voltage), and sweeping pattern. On the other hand, FCD is determined by the characteristic temperature limits beyond which the quality of the fiber is altered. These temperature limits can be considered intrinsic because they reflect such fiber properties as the defect density, impurities, alignment, and so forth. Therefore, FCD is a better quantity for characterizing the CCC of wires. Unfortunately, all previously reported CCC values for aligned buckypapers,[15] carbon fibers,[15] and CNT fibers[15,16] are MCDBB values. The FCD value for the particular case shown in Figure 1c is $1.03 \times 10^8$ A m$^{-2}$, while the MCDBB is $\approx 1.4 \times 10^8$ A m$^{-2}$.

© 2014 WILEY-VCH Verlag GmbH & Co. KGaA, Weinheim

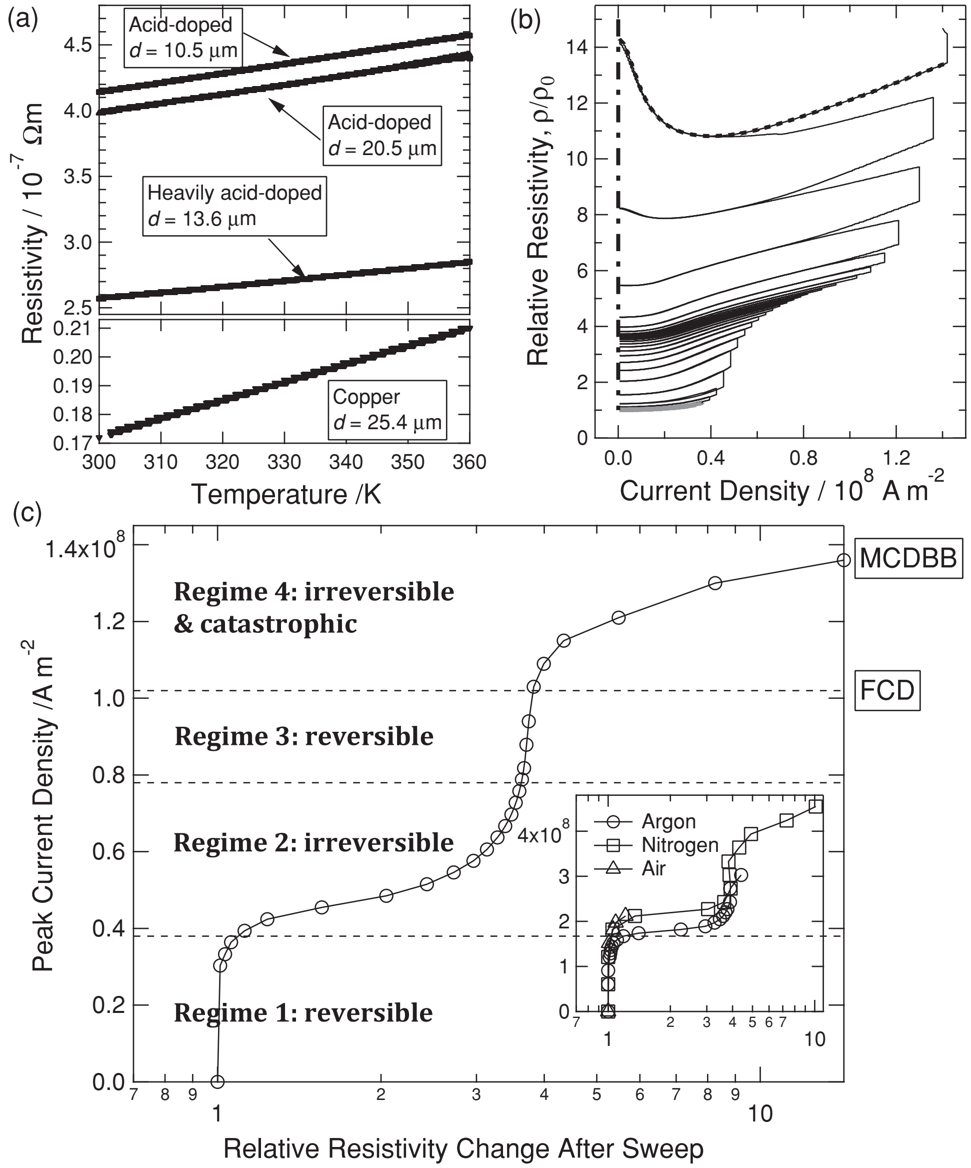

**Figure 1.** a) Resistivity versus temperature from room temperature to 360 K for the highly conductive carbon nanotubes fibers studied. The lowest curve is for the reference copper wire with a diameter of 25.4 μm. b) Resistivity versus current density for the 20-μm diameter, acid-doped CNT fiber in vacuum, showing hysteresis loops through a number of current-sweeping cycles described in the Experimental Section, indicating irreversible changes induced by the large currents. $\rho_0 = 3.98 \times 10^{-7}\ \Omega$ m is the initial resistivity. The bottom square curve indicates the first sweep point. The top dashed curve represents a typical curve in Regime 4. c) Peak current density applied in a current-sweeping cycle versus the low-current resistivity measured after the cycle. This graph shows four distinct regimes. The definitions of the maximum current density before breaking (MCDBB) and failure current density (FCD) are also indicated. The main panel is for data taken in vacuum and the inset shows data taken in argon, nitrogen and air.

### 2.2. Joule Heating Induced Annealing and Irreversible Change in *I–V* Curves

The data in Figure 1c provides significant insight into the mechanism by which the fiber leads to a catastrophic failure at high current densities. In Regime 2, a drastic irreversible process occurs, and the resistivity becomes about four times larger than the original value. Based on our modeling (see Supporting Information for detail), the maximum temperature of the fiber at the boundary between Regimes 1 and 2 is about 470 K, which is higher than the boiling point of chlorosulfonic acid (423 K). Therefore, we attribute the increase of resistivity in Regime 2 to an irreversible reduction of charge carriers through removal of chlorosulfonic acid, a p-type dopant. Even though Regime 2 is fairly narrow, the increase of resistivity significantly increases Joule heating. As a result, the finishing temperature (at the boundary between Regimes 2 and 3) is estimated to be about 1305 K.

Notably, the quality of the fiber is not degraded during the heating process in Regime 2, as confirmed by the maintained G/D ratio in Raman spectra (shown in Supporting Information). The fact that the *I–V* curve is reversible again in Regime 3

© 2014 WILEY-VCH Verlag GmbH & Co. KGaA, Weinheim

indicates that no chemical changes happen in this regime and the fiber is stable even though it is heated by high currents. Thus, we are essentially dealing with an annealed fiber in this regime, whose properties are different from those of the original, acid-doped fiber in Regime 1. Finally, as the average temperature exceeds about 1740 K, the fiber enters Regime 4, and the resistivity increases very rapidly, until it breaks.

A close examination of $\rho$–$i$ curves in Regime 4 provides further insight into the final moments when the fiber is breaking apart. Note that a typical curve in Regime 4, for example, the top dashed curve in Figure 1b, shows a qualitatively different trend than those in the other three regimes; that is, the resistivity initially decreases and then increases with increasing current density. This unusual trend can be explained only if we consider the general temperature dependence of resistivity of these fibers in a wider temperature range. Namely, with increasing temperature (from, e.g., 4.2 K), the resistivity initially decreases due to thermally-driven hopping transport and then increases due to intra-tube phonon-carrier scattering.[1] The crossover temperature ($T^*$), where the resistivity is minimal, is lower than the ambient temperature in the fibers we study here. This is why Equation 1 holds in the 300–360 K range. However, when the fiber starts breaking, the $\rho$–$T$ curve itself starts changing irreversibly and dynamically. Specifically, as the fiber starts structurally deteriorating, the hopping transport contribution becomes more and more important in determining the resistivity, which pushes $T^*$ higher and higher during the breaking process. The fact that we see an initial decrease in resistivity in Regime 4 (e.g., the top dash curve in Figure 1b) is evidence that $T^*$ has already become higher than $T_{\text{amb}}$. This is a self-intensified process because the initial damage forces a higher current through the remaining conductive paths, accelerating the breaking process.

### 2.3. Dependence of Failure Current on the Type of Surrounding Gas

The inset of Figure 1c shows that the type of gas surrounding the fiber critically affects the boundaries of different current regimes. In an argon or nitrogen gas environment, our CNT fibers exhibit qualitatively the same behavior as in vacuum, but the boundaries of regimes are shifted to much higher values. This is understandable because the gas contributes convective cooling, whereas in vacuum black-body radiation is essentially the only thermal path, except through the end contacts. On the other hand, fibers break more easily in air, usually breaking already in Regime 2; that is, the FCD value corresponds to the boundary between Regimes 1 and 2. We attribute this reduced FCD in air to the oxidation of carbon nanotubes, which can happen at temperatures between 773 and 873 K. The FCD values measured in different environments are summarized in **Table 1**.

It can be seen that the FCD values of the copper wire are still higher than those for the CNT fibers, mainly due to the lower resistivity of copper. However, the SFC values of the CNT fibers exceed copper wires' in all tested gases due to the much smaller mass densities of the CNT fibers. The dependence of FCD on the fiber dimensions as well as the surrounding medium are properly explained through our theoretical analyses (see Sections B and C of Supporting Information for detail; briefly, the FCD is proportional to $d^{-0.913}$ for a gas medium and $d^{-0.5}$ for a solid medium). These analyses also enable us to make a comprehensive comparison of CCC, mainly the MCDBB, with those numbers reported for other macroscopic CNT devices (see Section E of Supporting Information). The MCDBB value of this fiber is much higher than that of aligned buckypaper.[15] It is also higher than those reported for both a carbon fiber and CNT fiber[16] while it is similar to another reported value for a CNT fibril[17] (although the length of the sample was not specified). It is much smaller than a recently reported value $6 \times 10^{12}$ A m$^{-2}$ for a CNT-Cu composite, in which CNT occupies 45% volume fraction.[18]

**Table 1.** Failure current density (FCD), maximum current density before breaking (MCDBB), and specific failure current (SFC) values determined for an acid-doped carbon nanotube fiber with a diameter of 20.5 µm, through measurements in vacuum, argon, nitrogen, and air. The values in parentheses are the corresponding values estimated for copper (see Supporting Information for details on the estimations).

| | Vacuum | Argon | Nitrogen | Air |
|---|---|---|---|---|
| FCD [GA m$^{-2}$] | 0.103 | 0.273 | 0.330 | 0.182 |
| | | (0.912) | (1.135) | (1.135) |
| MCDBB [GA m$^{-2}$] | 0.136 | 0.303 | 0.455 | 0.211 |
| SFC [A m g$^{-1}$] | 85.0 | 225 | 272 | 150 |
| | | (66.3) | (82.5) | (82.5) |

The scanning electron microscopy images in **Figure 2** are further evidence that the type of surrounding gas affects the way the fiber breaks, also providing some clues about the breaking mechanisms. The break usually occurs in the middle of the fiber, where the local temperature is the highest, consistent with our simulations described in the next section (see **Figure 3**a). Some sharp, needle-like tips are seen at the breaking point, similar to earlier reports.[3,16,19] Tips observed in the fibers broken in vacuum, nitrogen, and argon are decorated by some ball-like clusters, whereas tips formed in the fiber broken in air are observed to be clean and free from such clusters. We hypothesize that these clusters are amorphous carbon or other carbon structures produced under high temperature. When the fiber breaks in air, the breaking mechanism is likely through oxidation, and the product is $CO_2$, so there is no amorphous carbon residual. However, in the other three cases (vacuum, argon, and nitrogen), the fiber breaks from the inside through current-induced heating that raises the temperature to the sublimation point. Thus, the generated amorphous carbon cannot escape to the outside quickly and remains at the breaking point.

### 2.4. Thermal Conductance between the Fiber and its Surrounding Gas

Since current-induced heating is the main cause of resistivity change in the fibers under high current densities, it is the balance between the heating current and the thermal dissipation into the surroundings that determines the detailed behavior of nonlinear $I$–$V$ curves. We have developed a model that can

© 2014 WILEY-VCH Verlag GmbH & Co. KGaA, Weinheim

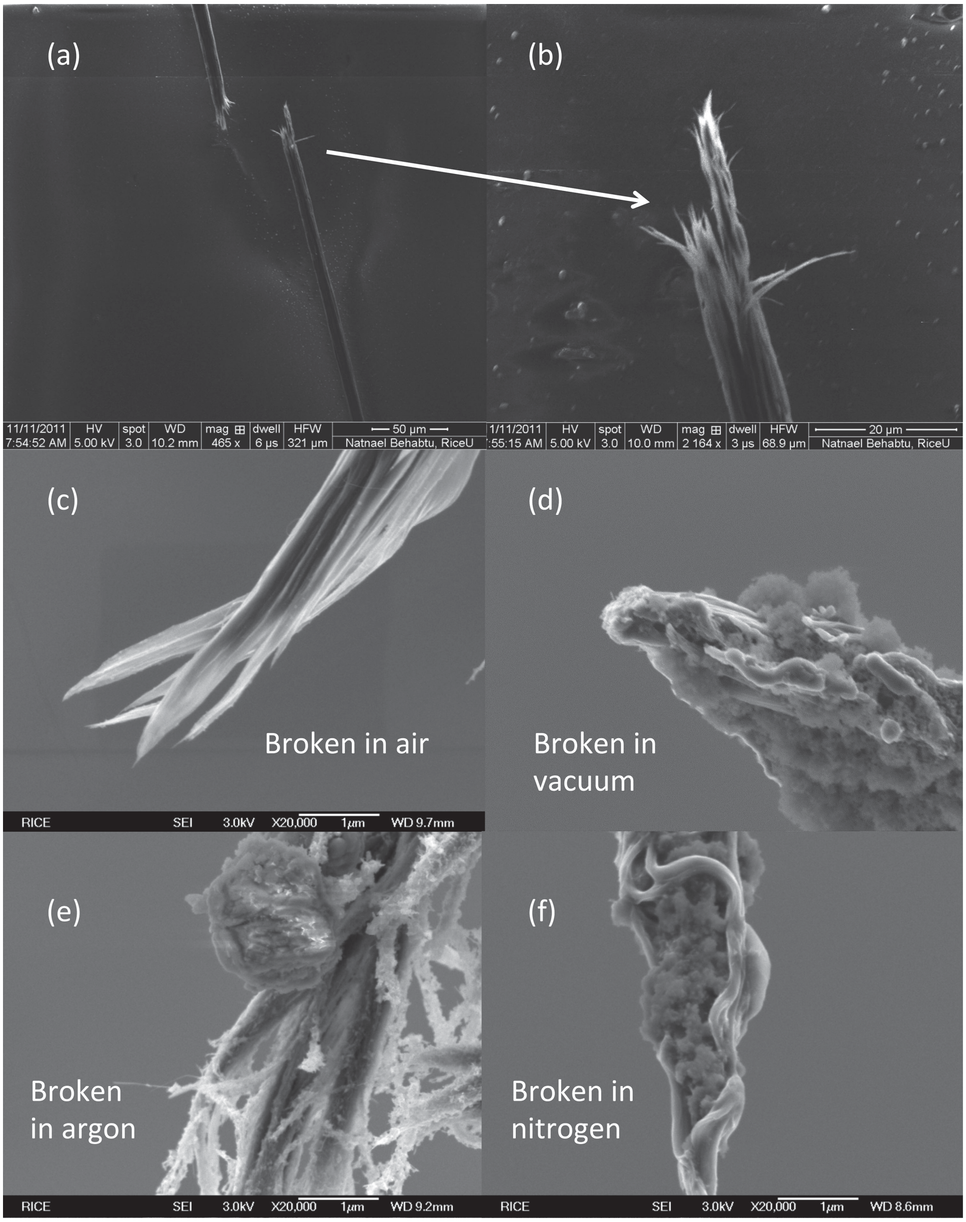

**Figure 2.** a,b): Scanning electron microscope images of a typical carbon nanotube fiber broken into two pieces in the middle due to high-current-induced Joule heating. Magnified images of the breaking point of fibers that were broken in c) air, d) vacuum, e) argon, and f) nitrogen.

make quantitative predictions and yield important parameters through fitting experimental data. Here we determine the thermal conductance, *g*, between the fiber and the surrounding gas through analysis of the nonlinear *I*–*V* in the reversible range (Regime 1) for the heavily acid-doped fiber in argon, nitrogen, and helium.

A current-carrying wire with finite length has a temperature distribution along the current direction, with the highest temperature in the middle of the wire and the lowest temperature at both ends (Figure 3a). The average temperature increase relative to the ambient temperature, $\Delta T_{\mathrm{avg}} = T_{\mathrm{avg}} - T_{\mathrm{amb}}$, of a current-carrying wire with length $L$ at a current density $i$ is given by

$$\Delta T_{\mathrm{avg}} = \Delta T_{\infty}\left\{1-\frac{\tanh(L/2L_{\mathrm{c}})}{L/2L_{\mathrm{c}}}\right\}+\Delta T_{\mathrm{end}}\frac{\tanh(L/2L_{\mathrm{c}})}{L/2L_{\mathrm{c}}}, \tag{2}$$

$$\Delta T_{\infty} = \frac{i^2\rho(T_{\mathrm{amb}})L_{\mathrm{c}}^2}{\kappa} \tag{3}$$

$$L_c \equiv \sqrt{\frac{\kappa d}{4g - i^2\rho(T_{\mathrm{amb}})d\alpha}} \tag{4}$$

where $T_{\mathrm{amb}} = 300$ K is the ambient temperature, $\Delta T_{\infty}$ is the temperature increase when the length is infinite ($L \to \infty$), $L_{\mathrm{c}}$ is the

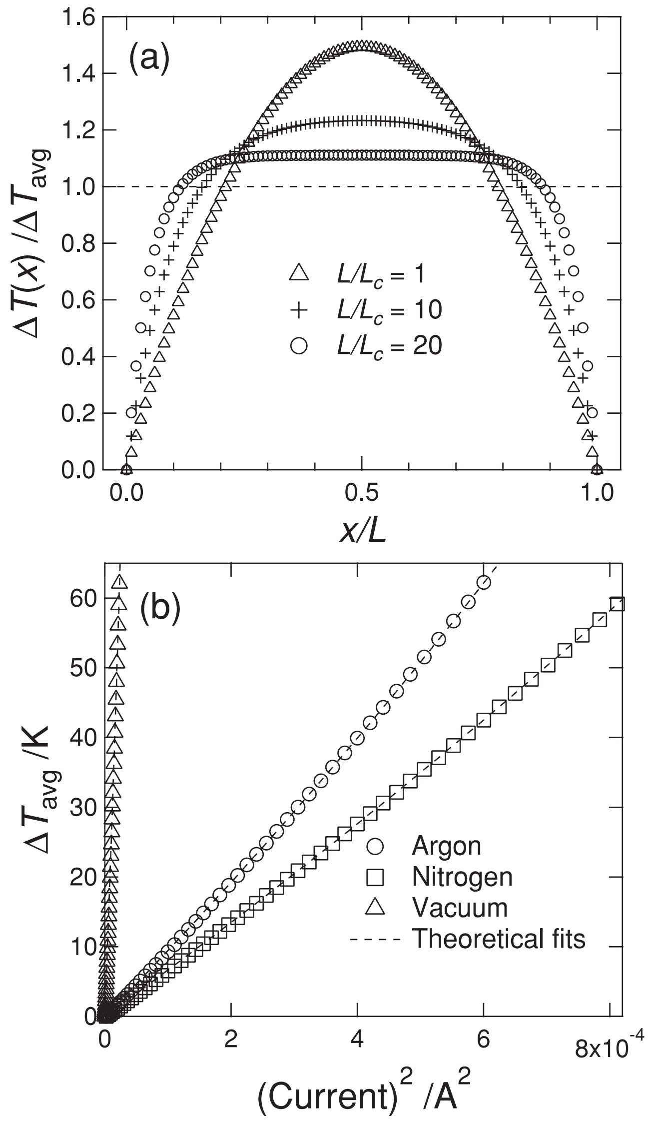

**Figure 3.** a) Temperature distribution in a current-carrying wire with finite length ($L$) with different critical thermal lengths ($L_c$), calculated based on a model described in Supporting Information. b) Measured average temperature increase of the heavily acid-doped CNT fiber as a function of the square of the applied current in vacuum, nitrogen, and argon. The dashed lines are theoretical fits based on Equation 2.

critical thermal length, $\kappa$ is the thermal conductivity of the wire at the ambient temperature (whose temperature dependence is very small in this temperature range), $\alpha$ is the temperature coefficient of $\rho(T)$ appearing in Equation 1, $d$ is the wire diameter, and $\Delta T_{\text{end}}$ is the temperature increase at the end contacts induced by the current. (see Section B of Supporting Information for details.)

In our experiments, we obtain both $\Delta T_{\text{avg}}$ and $\Delta T_{\text{end}}$ as a function of $i^2$ by converting the resistivities of the "AB" and "BC" portions, respectively, of the device (see **Figure 4**) into temperatures via Equation 1. Then, by fitting such data with Equation 1, we determine $\kappa$ and $g$. Particularly, under vacuum at a pressure of $10^{-5}$ Torr, heat transfer between the wire and gas can be ignored ($g = 0$), in which case the only fitting parameter is $\kappa$.

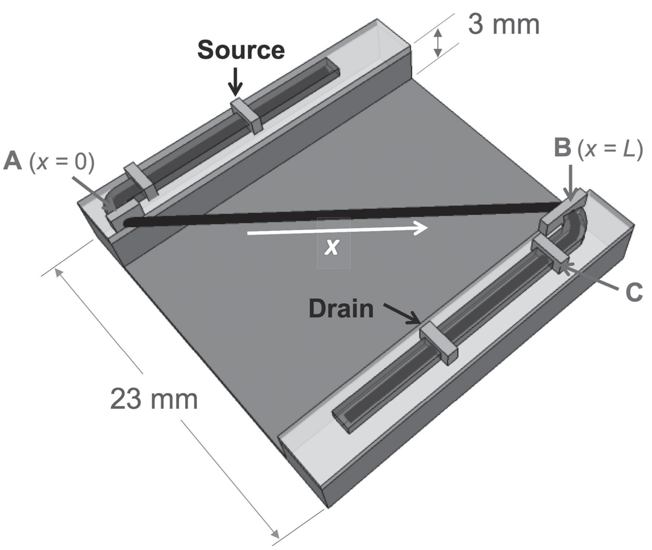

**Figure 4.** Schematic diagram for the experimental setup used in this work.

Figure 3b shows fitting results for $\Delta T_{\text{avg}}$ obtained for the heavily acid-doped CNT fiber in vacuum, argon, and nitrogen. The parameters extracted are listed in **Table 2**; the extracted $\kappa$ value is in good agreement with that reported earlier.[1]

Listed in the last two rows in Table 2 are estimates for the $g$ values for the 10.5-µm and 20.5-µm diameter CNT fibers based on natural convection theory (see Supporting Information), providing the correct orders of magnitude as well as the observed trends for $g$ with respect to the fiber diameter and gas type. In particular, we find that $g$ increases with decreasing $d$ ($g_{\text{gas}} \propto d^{-0.826}$), which in turn makes the CCC of smaller-diameter fibers larger, in agreement with the experimental data. Our results also show that CNT fibers possess similar $g$ values to copper wires, implying that the inner structure of the fibers is irrelevant to $g$, that is, any minimal gas flow into the body of the CNT fiber does not contribute to heat transfer. This fact supports the notion that our fibers consist of tightly-packed and well-aligned CNTs.

**Table 2.** Values for thermal conductance ($g$) between the current-carrying fiber and surrounding gas for the cases of helium, nitrogen, and argon, determined for carbon nanotube fibers and copper cable. $d$: fiber diameter. $\kappa$: thermal conductivity. The last two rows show estimates for CNT fibers with $d$ = 10.5 and 20.5 µm, respectively, from our model based on natural convection theory (see Supporting Information for detail).

| | $d$ [µm] | $\kappa$ [W m$^{-1}$ K$^{-1}$] | $g_{\text{helium}}$ [W m$^{-2}$ K$^{-1}$] | $g_{\text{nitrogen}}$ [W m$^{-2}$ K$^{-1}$] | $g_{\text{argon}}$ [W m$^{-2}$ K$^{-1}$] |
|---|---|---|---|---|---|
| Heavily acid-doped CNT fiber | 13.6 | 420 | 2973 | 571 | 395 |
| Acid-doped CNT fiber | 10.5 | 331 | 3689 | 716 | 494 |
| Acid-doped CNT fiber | 20.5 | 314 | 2007 | 379 | 260 |
| Copper wire | 25.4 | 423 | 2024 | 397 | 260 |
| Theoretical | 10.5 | | 3928 | 879 | 606 |
| Theoretical | 20.5 | | 2260 | 506 | 349 |

© 2014 WILEY-VCH Verlag GmbH & Co. KGaA, Weinheim

**Table 3.** Continuous current rating, $I^{\mathrm{CCR}}$ (mA), and the corresponding specific continuous current rating, $J^{\mathrm{CCR}} = I^{\mathrm{CCR}}/\lambda$ (A m g$^{-1}$), estimated for the CNT fibers and copper wire for an operating temperature of 363 K. The diameter $d$ (in µm) and linear mass density $\lambda$ (in $10^{-3}$ g m$^{-1}$) are also listed for each fiber.

| | $d$ | $\lambda$ | $I^{\mathrm{CCR}}_{\mathrm{helium}}$ | $I^{\mathrm{CCR}}_{\mathrm{nitrogen}}$ | $I^{\mathrm{CCR}}_{\mathrm{argon}}$ | $I^{\mathrm{CCR}}_{\mathrm{helium}}$ | $I^{\mathrm{CCR}}_{\mathrm{nitrogen}}$ | $I^{\mathrm{CCR}}_{\mathrm{argon}}$ |
|---|---|---|---|---|---|---|---|---|
| Heavily acid-doped fiber | 13.6 | 0.212 | 62.2 | 27.3 | 22.7 | 293 | 129 | 107 |
| Acid-doped fiber | 10.5 | 0.105 | 37.3 | 16.4 | 13.6 | 355 | 156 | 130 |
| Acid-doped fiber | 20.5 | 0.400 | 76.5 | 33.2 | 27.5 | 191 | 83.1 | 68.8 |
| Copper wire | 25.4 | 4.54 | 482 | 214 | 173 | 106 | 47.0 | 38.1 |

### 2.5. Estimation of the Continuous Current Rating (CCR)

With the above determined values for $g$, together with the temperature-dependent resistivity, Equation 1, we can now calculate the CCR values for the CNT fibers for any assumed operating temperature in the reversible current region, $T_o$. As an example, here we show the calculated CCR for infinitely long CNT fibers at $T_o = 363$ K. By setting $\Delta T_\infty = T_o - T_{\mathrm{amb}}$ in Equation 3, we can derive the following compact expression for calculating CCR:

$$I^{\mathrm{CCR}} = \sqrt{\frac{\pi^2 d^3 (T_o - T_{\mathrm{amb}})\, g}{4\rho(T_o)}} \tag{5}$$

Note that with $g \propto d^{-0.826}$, we can predict that $I^{\mathrm{CCR}} \propto d^{1.087}$. The specific CCR is then given as $J^{\mathrm{CCR}} = I^{\mathrm{CCR}}/\lambda$, where $\lambda$ is the linear mass density (in kg m$^{-1}$) of the cable. **Table 3** lists the obtained $I^{\mathrm{CCR}}$ and $J^{\mathrm{CCR}}$ values for our CNT fibers and the reference copper wire for $T_o = 363$ K and $T_{\mathrm{amb}} = 303$ K. Again, the specific CCR values of CNT fibers are comparable to or larger than that of the copper wire. The current densities corresponding to these CCR values are 2–5 × $10^8$ A m$^{-2}$ for the 10-µm fiber and 1–2 × $10^8$ A m$^{-2}$ for the 20-µm fiber.

## 3. Conclusion

We characterized the current-carrying capacity, CCC or ampacity, of highly-conductive carbon nanotube fibers by measuring both their failure current density, FCD, and continuous current rating, CCR, based on a systematic study of their DC transport performance over a broad current range. We first demonstrated that there are four distinct regimes as we gradually increase the current density toward the breaking point; we provided qualitative explanations for the different regimes. The measured FCD values ranged from $10^7$ to $10^9$ A m$^{-2}$, depending on the diameter as well as the environmental gas type. The measured FCD in vacuum was the lowest due to lack of heat exchange with gases, while the measured FCD in air was smaller than in the other tested gases because of oxidation. In addition, we theoretically analyzed the heat exchange between CNT fibers and each type of gas, successfully extracting the thermal conductance between them. Furthermore, our results indicated that the tight packing and good alignment of our CNT fibers are crucial for obtaining the large CCC values. The FCD of our fibers is higher than previously reported carbon fibers and CNT fibers. If normalized by the linear mass density, both the specific failure current and specific continuous current rating of these CNT fibers exceed those of the copper wire. The combination of high specific CCC and good mechanical strength of our CNT fibers makes them promising candidates for power transmission cables.

## 4. Experimental Section

*Sample Preparation*: CNT fibers were produced by wet spinning.[1] Purified CNTs were dissolved in chlorosulfonic acid at a concentration of 3 wt% and filtered to form a spinnable liquid crystal dope.[20] The dope was then extruded through a spinneret (65–130 µm in diameter for different diameter fibers) into a coagulant (acetone or water) to remove the acid. The forming filament was collected onto a winding drum with a linear velocity higher than the extrusion velocity to enhance the alignment. The produced fibers were further washed in water and dried in an oven at 115 °C. Such fiber is called an acid-doped fiber. Thermal gravimetric analysis (TGA) shows that there still remains about 7 wt% of acid residuals in the acid-doped fiber.[1] On the other hand, if the produced fibers were first dried in an oven at 115 °C and then washed in water, there would be even more acid residuals in the fiber. Such fiber is called a heavily acid-doped fiber. Based on the linear density difference between the heavily acid-doped fiber and the acid-doped fiber, these fibers contain 9–16 wt% acid. The acid-doped fibers were stored in air for two years, and their resistivities did not change with time. The heavily acid-doped fiber was produced one month before the experiments were performed, and thus, no information is available on its long-term stability. In some cases, excessive acid doping made the room temperature resistivity as low as 1.7 × $10^{-7}$ Ω m, but after annealing at 373 K in vacuum for 12 h, this value quickly returned back to about 2.5 × $10^{-7}$ Ω m and became stable. Thus, the temperature range in which a fiber can be operated without any irreversible property change must be taken into consideration for specific applications. The 99.99% pure copper wire with 0.001 inch diameter was purchased from ESPICorp, Inc.

*Experimental Setup*: A copper substrate with a wide river bed and two narrow river banks was used to hang the cable (either a CNT fiber or copper wire) as shown in Figure 4. The depth of the bed was ≈3 mm and the width ≈23 mm. The cable was bent into a Z-turn with its mid-section suspended over the river bed.

© 2014 WILEY-VCH Verlag GmbH & Co. KGaA, Weinheim

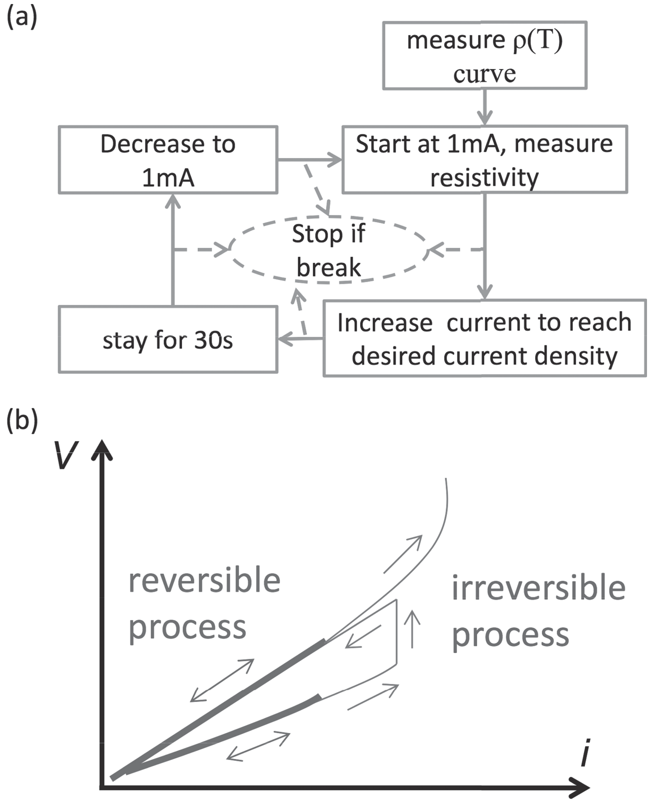

**Figure 5.** Experimental procedure for studying high-field DC transport to determine the CCC of CNT fibers. a) Flow chart describing the procedure step-by-step. b) Schematic diagram showing reversible and irreversible processes in a current-sweeping cycle.

Each arm was placed on a thin (100 µm) electrically-insulating quartz slide, which was itself placed on the river bank. Several silver epoxy electrodes (≈0.5 mm wide) were placed on the fiber for resistivity measurements. In particular, two electrodes (denoted by A and B in Figure 4) were placed at the ends of the suspended portion of the cable. Electrode C was placed 2 mm away from electrode A and B, and BC serves as a local probe to monitor the resistivity change at the end of the suspended fiber. The whole device was assembled on a vacuum-sealed heating-cooling stage in which the temperature of the device and the gas environment could be adjusted.

The experimental procedure is shown in the flow chart in **Figure 5**a. First, the sample is uniformly heated up and cooled down by the heating-cooling stage, while the resistivity of the AB section is measured as a function of temperature (see Figure 1a). Then a current sweep is carried out in high vacuum ($10^{-5}$ Torr), in one of four dry gases (nitrogen, helium, argon, and air) at atmospheric pressure, or on an intrinsic silicon substrate in air. In this step, the current is gradually swept up to reach the desired current density, held for 30 s, and then gradually swept down to 1 mA (see Figure 5a). The experiment is halted if the fiber breaks. If the electrical properties of the fiber are unchanged by current sweeping, the *I–V* curves from all sweeping cycles show no hysteresis (Figure 5a, thick curve), but if they are changed, the *I–V* curve will initially follow the sweeping-down curve of the previous circle and then start to deviate (Figure 5b, thin curve). Since the fiber might not be homogeneously Joule heated, the extracted resistivity is an average value given by

$$\bar{\rho}_f(i)=\frac{V_f}{i l_f} \qquad (6)$$

where $i$, $V$, and $l$ are the current density, voltage, and length of the cable with $f$ = AB and BC representing the measured section (see Figure 4).

## Acknowledgement

This work was supported by the Department of Energy (through Grant No. DE-FG02–06ER46308), the National Science Foundation (through Grants No. OISE-0530220 and EEC-0540832), the Robert A. Welch Foundation (through Grant Nos. C-1509 and C-1668), Teijin Aramid BV, Tei-jin Techno Products Ltd., Air Force Office of Scientific Research FA9550–09–1–0590, and the U.S. Department of Defense National Defense Science and Engineering Graduate Fellowship.

Received: November 14, 2013
Revised: December 30, 2013
Published online: February 13, 2014

---

[1] N. Behabtu, C. C. Young, D. E. Tsentalovich, O. Kleinerman, X. Wang, A. W. K. Ma, E. A. Bengio, R. F. ter Waarbeek, J. J. de Jong, R. E. Hoogerwerf, S. B. Fairchild, J. B. Ferguson, B. Maruyama, J. Kono, Y. Talmon, Y. Cohen, M. J. Otto, M. Pasquali, *Science* **2013**, *339*, 182–186.

[2] P. Jarosz, C. Schauerman, J. Alvarenga, B. Moses, T. Mastrangelo, R. Raffaelle, R. Ridgley, B. Landi, *Nanoscale* **2011**, *3*, 4542–4553.

[3] Y. Wei, K. Jiang, L. Liu, Z. Chen, S. Fan, *Nano Lett.* **2007**, *7*, 3792–3797.

[4] P. T. Murray, T. C. Back, M. M. Cahay, S. B. Fairchild, B. Maruyama, N. P. Lockwood, M. Pasquali, *Appl. Phys. Lett.* **2013**, *103*, 053113.

[5] Z. Yao, C. L. Kane, C. Dekker, *Phys. Rev. Lett.* **2000**, *84*, 2941–2944.

[6] B. Q. Wei, R. Vajtai, P. M. Ajayan, *Appl. Phys. Lett.* **2001**, *79*, 1172–1174.

[7] P. G. Collins, M. Hersam, M. Arnold, R. Martel, P. Avouris, *Phys. Rev. Lett.* **2001**, *86*, 3128–3131.

[8] M. Hauder, J. Gstottner, W. Hansch, D. Schmitt-Landsiedel, *Appl. Phys. Lett.* **2001**, *78*, 838–840.

[9] M. A. Kuroda, A. Cangellaris, J.-P. Leburton, *Phys. Rev. Lett.* **2005**, *95*, 266803.

[10] J. Y. Huang, S. Chen, S. H. Jo, Z. Wang, D. X. Han, G. Chen, M. S. Dresselhaus, Z. F. Ren, *Phys. Rev. Lett.* **2005**, *94*, 23680.

[11] K. Mølhave, S. B. Gudnason, A. T. Pedersen, C. H. Clausen, A. Horsewell, P. Bøggild, *Nano Lett.* **2006**, *6*, 1663–1668.

[12] Y. Wei, P. Liu, K. Jiang, L. Liu, S. Fan, *Appl. Phys. Lett.* **2008**, *93*, 023118.

[13] Fink, D. G., H. W. Beaty, Standard Handbook for Electrical EngineersMcGraw-Hill Professional, New York **2006**.

[14] G. J. Anders, Rating of Electric Power Cables: Ampacity Computations for Transmission, Distribution, and 7ndustrial Applications IEEE Press Power Engineering Series; McGraw-Hill, New York **1997**.

[15] J. G. Park, S. Li, R. Liang, X. Fan, C. Zhang, B. Wang, *Nanotechnology* **2008**, *19*, 185710.

[16] L. Song, G. Toth, J. Wei, Z. Liu, W. Gao, L. Ci, R. Vajtai, M. Endo, P. M. Ajayan, *Nanotechnology* **2012**, *23*, 015703.

[17] Y. Zhao, J. Wei, R. Vajtai, P. M. Ajayan, E. V. Barrera, *Sci. Rep.* **2011**, *1*, 83.

[18] C. Subramaniam, T. Yamada, K. Kobashi, A. Sekiguchi, D. N. Futaba, M. Yumura, K. Hata, *Nat. Commun.* **2013**, *4*, 2202.

[19] F. Ding, K. Jiao, Y. Lin, B. I. Yakobson, *Nano Lett.* **2007**, *7*, 681–684.

[20] V. A. Davis, A. N. Parra-Vasquez, M. J. Green, P. K. Rai, N. Behabtu, V. Prieto, R. D. Booker, J. Schmidt, E. Kesselman, W. Zhou, H. Fan, W. W. Adams, R. H. Hauge, J. E. Fischer, Y. Cohen, Y. Talmon, R. E. Smalley, M. Pasquali, *Nat. Nanotechnol.* **2009**, *4*, 830–834.

© 2014 WILEY-VCH Verlag GmbH & Co. KGaA, Weinheim